JOURNAL OF MATERIALS SCIENCE 31 (1996) 4369–4374

Study of the porous structure of hardened gypsum by pulsed nuclear magnetic resonance

A. V. FILIPPOV, M. G. ALTYKIS, M. I. KHALIULLIN, R. Z. RACHIMOV, V. M. LANTSOV
Department of Physics, Kazan Civil Engineering Institute Zelenaya Str. 1, Kazan, 420043, Russia

The porous structure of hardened gypsum prepared by hydration of $CaSO_4 \cdot 0.5H_2O$ and $CaSO_4$ was studied by nuclear magnetic resonance. The combined analysis of the melting curves of water confined in pores, the shapes of diffusional echo attenuations and dependencies of apparent self-diffusion coefficients of water and olygomer confined in pores on diffusion time, shows that the porous geometry of the hardened gypsum prepared from calcium hemihydrate and anhydrite can be represented by a model of randomly oriented layers. In the case of hemihydrate, most of the pores are arranged in the macropores range. In the case of pure anhydrite, the fraction of macropores is about 90% and diminishes to 30% as a result of modification. The rest of the pores (10%–30%) are arranged in the mesopores range. This has been established for the first time for the hardened gypsum. The length of pores along the layer was also estimated. In the case of hemihydrate, this value was more than 2.5×10^{-5} m, and in the case of anhydrite it was about 0.5×10^{-6} m. It is found that the use of modifiers results in a decrease in the layer thickness and permeability of the hardened gypsum.

1. Introduction

The physical, mechanical and chemical properties of porous substances are determined to a great extent by pore structure (distribution, geometry, etc.). This is also important for construction materials where characteristics of pores often influence the final properties of the product (durability, water resistance, heat and sound conductivity, strength).

The porous structure of hardened gypsum was studied by electron microscopy and mercury porosimetry methods [1–5]. It was shown that it depended on the dispersion of raw material, water to binder ratio, temperature, employment of modifiers, etc. The shape of the crystallites can be needle-like or layer-like [2, 3], depending on the magnitudes of the above-mentioned factors and their combination. The pores are interconnected, their average dimensions are more than 5×10^{-8} m according to Brukner [1], or from 1.3×10^{-6} to 4.5×10^{-6} m according to Lack [3]. i.e. they can be classified as macropores (larger than 5×10^{-8} m [6]).

Radiospectroscopy methods have been widely used during the last few years, together with the conventional methods in the investigation of porous structure. One of these method is nuclear magnetic resonance (NMR). Several NMR investigations on hardened cement paste have been carried out during the last few years, in which the porous structure of artificially hardened materials was studied [7–9]. As far as we know, no similar investigations have been carried out on hardened gypsum until now, except for our earlier work [10].

In the present work, NMR was used to study the porous structure, firstly through the analysis of the dependence of liquid water fraction in pores versus temperature, and secondly, through the analysis of self-diffusion of liquid molecules (water or olygomer) in pores.

In the first case, the parameters of pore-size distribution were determined from the temperature dependence of the relative volume of the liquid pores.

In the second case, the molecules of confined liquid are used as a probe, yielding information about the geometry of the porous media. The influence of porous media on the self-diffusion coefficient of a confined liquid was considered in a number of works on fractals [11], and has been investigated experimentally in samples with well-defined structure [12–14]. In several works, attempts were made to estimate the characteristics of the porous structure through the analysis of the shape of the diffusional echo attenuation [10, 15, 16].

In the present study, samples of hardened gypsum prepared by hydration of $CaSO_4 \cdot 0.5H_2O$ and $CaSO_4$ without and with some modifiers that reduce water-resistance and enhance the compression strength of the resulting product, were used. The purpose of this work was to determine the characteristics of the porous geometry of hardened gypsum and to elucidate the effect of binder composition on porous structure.

0022–2461

2. Experimental procedure

2.1. Materials

We have investigated five samples of hardened gypsum with the matrix composed of $CaSO_4 \cdot 2H_2O$. Samples 1 and 2 were prepared by hardening of $CaSO_4 \cdot 0.5H_2O$ (hemihydrate, HH), without the additives (sample 1) and with them (sample 2). The starting material for the other samples (3–5) was $CaSO_4$ (anhydrite, AH), without additives (sample 3) and with them (samples 4 and 5). The additives used were a hydration activator (earthy gypsum), a superplasticizer and fillers. The product of the condensation of naphthalene sulfonic acid with formaldehyde was used as the superplasticizer [17]. Sample compositions and their compressive strength are presented in Table I. The duration of the hardening process was about one day (for samples 1 and 2) and 28 days (samples 3–5) at room temperature which was appropriate to completion of the process of hydration and the formation of a porous structure [5]. The specific surface determined by the BET method is about $1\ m^2\ g^{-1}$ for all the samples. We could not determine any differences between the samples by this method.

A self-diffusion study was carried out on water- and olygomer-saturated samples. Before the injection of olygomer, the samples were carefully dried under vacuum at 50 °C for 4 h. The olygomer used was polypropylene oxide (PPO) with $M = 1025$, $M_w/M_n \simeq 1.1$.

Before describing the experimental methods used, various notations are explained. The definition of pore size in the case of non-spherical pore is not unambiguous. In this case, irrespective of the pore shape, we can introduce at least two parameters, which can be understood in the most simple and objective way. These are minimal, d_{min}, and maximal, d_{max}, dimensions, corresponding to minimal and maximal distances between the walls of the pore, respectively. These parameters are usually called pore diameter and pore length.

2.2. The decrease of water melting temperature in pores

The liquid confined inside the pore is characterized by a lowered melting temperature. The formation of a small crystal has been treated theoretically by Gibbs [18] and Thomson (Kelvin) [19] who showed the effect of surface curvature on the equilibrium state of a pure substance. According to both Gibbs and Thomson the equation describing the dependence of melting-point depression for a crystal of dimension d on thermodynamic parameters is given by

$$\Delta T = 4\sigma T^0/d\Delta H\rho_c \quad (1)$$

were σ is the surface energy of solid-liquid interface, T^0 is the normal bulk melting point, ΔH is the bulk enthalphy of fusion, $\Delta T = T^0 - T_m$, T_m is the melting temperature, ρ_c is the density of solid. It is clear, that maximum ΔT corresponds to minimum d. Consequently, the melting of a crystallite of complicated shape is determined by the minimal distance between the pore walls (pore diameter).

The dependence of melting temperature on pore diameter has been well studied experimentally [20–24]. As a result, the dependence of ΔT on d_{min} for a number of porous substances and confined liquids, were determined. It was shown that, in the case of the water, ΔT is determined only by the size of the pore, and not by the nature of the porous medium [21].

One of the most suitable methods to determine the melting point in porous media is nuclear magnetic resonance [22–24]. Recently, Strange and co-workers proposed the use of this method in combination with the depression of melting point in pores as a novel method to determine pore-size distribution [23, 24]. The use of cyclohexane instead of water, the most popular absorbent, and automatic collection of data, enabled the authors to increase the sensitivity of the method, and to determine pore diameter distributions for a number of porous silica.

We have used a variation of the method proposed by Strange and co-workers, with two changes. Firstly, we used water as the natural absorbent of hardened gypsum materials. Secondly, we analysed free induction decays instead of the spin-echo amplitudes. This is caused by the dependence of the transverse NMR relaxation time upon the pore diameter, a fact which can lead to the distortion of the ratio of echo amplitudes of liquids confined in pores of different diameters. The curve of water melting in porous glasses with a narrow distribution of pore size, was used as a calibration curve [22]. We have verified the method by investigating the melting of ice in carbon cylindrical pores with a narrow diameter distribution [25]. The sizes, determined in this experiment, appeared to coincide well with those obtained by adsorption.

The NMR relaxation of water protons was studied on a home-built spectrometer with resonance ^1H frequency 20 MHz. Free induction decay is given by

$$A(t) = P_1 f_1(t) + P_2 f_2(t) \quad (2)$$

where t is the time, $f_1(t)$ corresponds to the relaxation of protons of crystallohydrate, ice and adsorbed water, $f_2(t)$ corresponds to relaxation of "liquid" water protons, P_1 and P_2 are the proton populations. $f_1(t)$ and $f_2(t)$ are characterized by NMR relaxation times of about 10 μs and more than 1 ms, respectively. The relative fraction of liquid water at temperature, T, was

TABLE I Compositions of raw material (wt %) used for preparing hardened gypsum, and the compressive strengths of the final product

Components	Sample				
	1	2	3	4	5
$CaSO_4 \cdot 0.5H_2O$	100	90.5	–	–	–
$CaSO_4$	–	–	95	87	78.75
Water-to-binder ratio	51	35	34.5	23.5	24.5
Quartz sand	–	2.5	–	15	15
Lime	–	5	5	5	5
Earthy gypsum ($CaSO_4 \cdot 2H_2O$)	–	1	–	2	–
Superplasticizer	–	1	–	1	1
$Al_2(SO_4)_3$	–	–	–	–	0.25
Compressive strength (MPa)	12	30	31.5	50	45

determined from the relation

$$C(T) = P_2(T)/P_2(T = 0\,^{\circ}\mathrm{C}) \quad (3)$$

In order to raise the precision of melting temperature determination, to exclude the effect of surface water and to reduce temperature gradient along the sample, the experimental procedure was improved in the following ways.

1. The spectrometer was equipped with a high-precision temperature-control sample unit ($\approx 0.2\,^{\circ}\mathrm{C}$).

2. All samples after saturation were washed in CCl_4 in order to remove surface water.

3. Samples were placed in CCl_4 filled glass tubes. A gap was left between tube walls and the sample for CCl_4 convection.

4. Nitrogen vapour, which was used as the heat carrier, was pumped from the top to the bottom of the tube.

2.3. Self-diffusion of liquid molecules confined in pores

The detailed description of the pulsed-field gradient method (PFG) can be found elsewhere [26, 27]. The application of this method to the study of porous substances is discussed in numerous publications, for example [12–16]. The molecules of liquids, in the absence of temperature and concentration gradients, participate in translational motion. The root mean square displacement of the molecules (RMD, $|r|$) for a bulk liquid is the Gaussian random process with propagator (normalized probability that a molecule shifts to the distance $|r|$ in the direction of the pulsed-gradient vector during the time interval t_d)

$$P(|r|, t_d) = (4\pi D_0 t_d)^{-3/2} \exp[-\langle r^2\rangle/(4D_0 t_d)] \quad (4)$$

In this case, Einsteins equation for RMD holds

$$\langle r^2\rangle = 6D_0 t_d \quad (5)$$

where D_0 is the self-diffusion coefficient (SDC) of the molecules in bulk liquid. D_0 does not depend on the diffusion time and is characteristic of the molecular translational motion.

The diffusional echo-attenuation (EA) detected in the PFG experiment is the Fourier transformation of $P(|r|, t_d)$ and, in the case of bulk liquid, is given by

$$A(g^2)/A(0) = \exp(-kD_0) \quad (6)$$

where $A(g)$ is the spin-echo amplitude, $k = \gamma^2\delta^2 g^2 t_d$, γ is the gyromagnetic ratio, δ and g are duration and amplitude of the gradient pulse, respectively.

For the liquid confined in pores, the statistics of molecular RMD are determined by the morphology of the porous medium. The shape of EA often differs from Equation 6. In these cases, the most convenient physical characteristics of translational motion is apparent SDC ($\langle D\rangle$)

$$\langle D\rangle = -(\gamma^2\delta^2 t_d)^{-1} \frac{\partial\{\ln[A(g)]\}}{\partial(g^2)}\Big|_{g\to 0} \quad (7)$$

As t_d increases, the following typical cases can be considered.

1. In the range of small diffusion times, when RMD is small relative to pore size, $\langle D\rangle$ is close to D_0. The shape of EA is similar to Equation 6.

2. As t_d increases, when $|r| \sim d_{min}$ the transitional regime for translational diffusion is achieved. The dependence of $\langle D\rangle$ on t_d is observed and EA becomes non-exponential. Mitra *et al.* showed that the slope of this dependence is given by [14]

$$\frac{\langle D\rangle}{D_0} \sim 1 - \frac{4(D_0 t_d)^{0.5}}{9(\pi)^{0.5}} \frac{S}{V} \quad (8)$$

where S and V are pore surface area and pore volume, respectively.

3. In the range of sufficiently large $t_d(|r| > d_{max})$, $\langle D\rangle$ attains the constant effective value, D_{eff}. The relation D_{eff}/D_0 characterizes the permeability of the media for molecules of the liquid and is closely connected with such properties of substance as sound and heat permeability, and electrical conductivity.

4. Finally, when RMD becomes comparable with the correlation length of the porous medium, ζ, in accordance with the central limits theorem of probability theory, the averaging of translational motion over large number of random orientations leads to the fulfillment of the Gaussian statistics for the displacements. EA is described by Equation 6 with the SDC equal to D_{eff}. In the experiment, the beginning of such averaging can be detected from a tendency of the EA shape to change into exponential form when t_d increases.

The PFG experiments were performed using the NMR spectrometer built by the venture "Magnitnyi Resonans" [28], operating at the ^1H frequency of 60 MHz. In our experiments, g was varied from 0 to maximal value at constant δ and t_d. The maximum value of g was $40\ \mathrm{T\,m^{-1}}$. The "stimulated echo" pulse sequence was used.

3. Results and discussion

The dependences of the volume fractions of pores on pore diameters derived from the melting point depression are shown in Fig. 1. It is seen that pore diameter distributions (PDD) of samples studied are rather broad and differ for all samples studied. The peak of PDD in pure HH is situated in the region of large pore diameters, beyond the resolving power of this method (curve 1). In samples, 2–5, most of the pores are characterized by diameters less than 100×10^{-9} m (curves 2–5). It is obvious that, in samples 1 and 2 (HH), the number of pores with diameters less than 5×10^{-8} m (mesopores) is rather small. The peak in pure AH is situated in the range around 80×10^{-9} m (curve 3). In this case the fraction of mesopores is about 0.1 only. The use of modifiers leads to the shift of peaks of both HH and AH into the region of small pore diameters (curves 2, 4, 5). For sample 4 two peaks of the distribution probably exist (curve 4). Sample 5 shows a minimum pore diameter (curve 5). In samples 4–6, the fraction of mesopores is greater than 0.65.

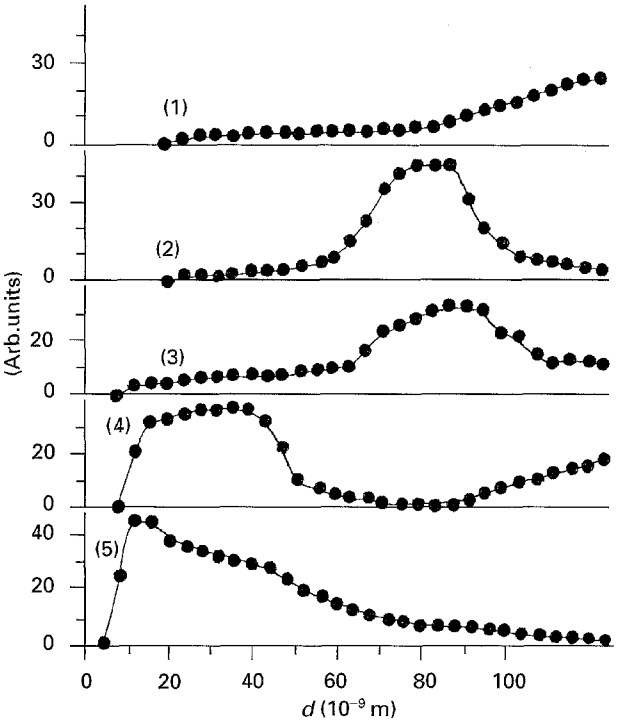

Figure 1 Pore diameter distributions in samples (1) 1, (2) 2, (3) 3, (4) 4 and (5) 5.

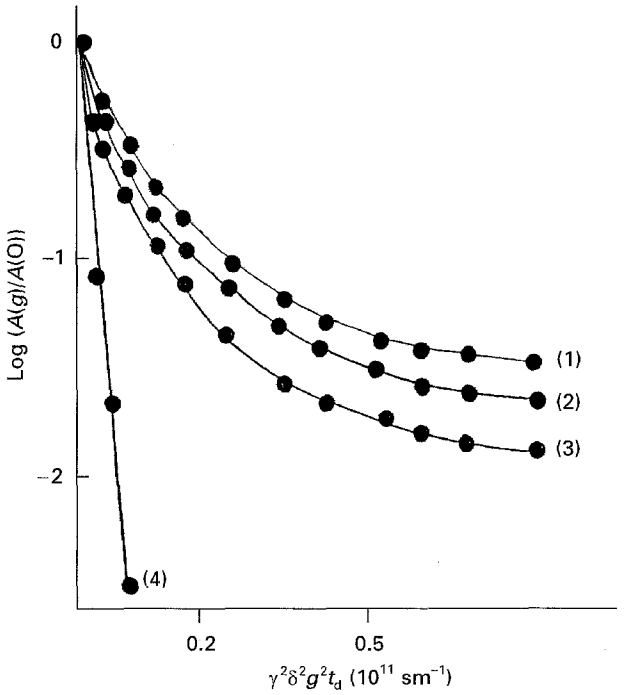

Figure 2 The diffusional echo-attenuations as a function of g^2 for sample 1 at diffusion times of (1) 4 ms, (2) 20 ms, (3) 100 ms and (4) for bulk water.

Echo-attenuations for water molecules confined in pores, which are typical for all systems under study, are shown in Fig. 2. These EA are non-exponential. However, with the use of scaling of the x-axis of the plot, we can superimpose the initial parts of all EA. As a result of this procedure, all EA coincide and form one curve [10]. This curve can be described by the analytical expression derived for self diffusion of the

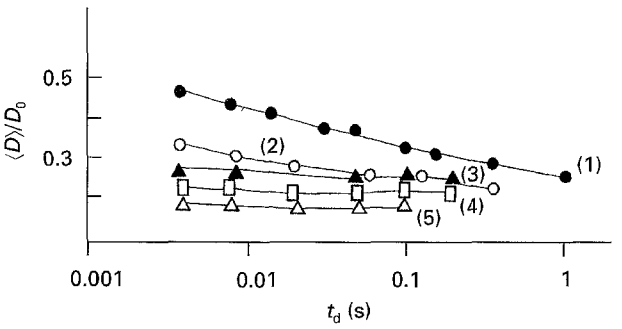

Figure 3 The dependencies of the ratio $\langle D\rangle/D_0$ for water molecules as a function of diffusion time for samples (1) 1, (2) 2, (3) 3, (4) 4 and (5) 5 at 30 °C.

TABLE II Characteristics of the samples determined from plots $\langle D\rangle$ (t_d)

Sample	$(D_{eff}/D_0)_{H_2O}$	$(D_{eff}/D_0)_{PPO}$	V/S (μm)
1			4.00
2			1.10
3	0.24	0.29	0.74
4	0.22	0.24	0.72
5	0.20	0.20	0.57

molecules in the layers randomly oriented with respect to the pulsed-field gradient [15]

$$A(g)/A(0) = \exp(-kD_i)\int_0^1 \exp(k_0 D_i x^2)\mathrm{d}x \quad (9)$$

where D_i is the apparent interlayer SDC.

The plots of ratios of the apparent SDC of water confined in pores of samples 1–5 to the SDC of bulk water ($D_0 = 2.7\times10^{-9}$ m^2 s^{-1}) versus t_d are shown in Fig. 3. The ratio $\langle D\rangle/D_0$ for all of the samples is much less than unity. The time dependence of $\langle D\rangle$ for AH is virtually absent (curves 3–5). For HH, the observed $\langle D\rangle(t_d)$ dependence is typical for a transitional regime (curves 1 and 2). The independence of $\langle D\rangle$ from t_d shows that in AH in the range of experimental t_d, interporous diffusion takes place, i.e. $\langle D\rangle$ represents D_{eff}. The values of D_{eff}/D_0 can be used to characterize the sample's permeability in the length scale of observed RMD of water molecules. These values are presented in Table II.

The RMD of water molecules for $t_d = 4$ and 100 ms, estimated from Equation 5, are $\simeq 5\times10^{-6}$ and $\simeq 2.5\times10^{-5}$ m, respectively. We cannot investigate self diffusion at smaller displacements because of the technical limitations of the apparatus (minimum t_d is 1 ms). One way to solve this problem is to substitute water by another liquid, with SDC smaller than that of water [10]. It is evident from Equation 5 that in order to decrease RMD, for example, by one decimal order, D_0 of this liquid should be 100 times smaller than that of water molecules. The additional requirements are as follows: the size of the molecules should be sufficiently small to penetrate into even the smallest pores, and liquid should not damage pore walls. We used PPO olygomer as such a liquid. The root mean square end-to-end distance, which was taken as the

size of the PPO molecule, was the size of Kuhn's segment [29] and is 1.1×10^{-9} m. This value is essentially smaller than the pore diameters of the samples studied (see [1] and data in Fig. 1). The measurements were performed at 10 °C. D_0 of the bulk PPO at this temperature is 7.2×10^{-12} m^2 s^{-1}.

In Fig. 4 the $\langle D \rangle / D_0$ plots for PPO in samples 1–5 are shown as the function of t_d. The RMD values, derived according to Equation 2 at $t_d = 4$ ms and 100 ms are $\simeq 0.4 \times 10^{-6}$ m and $\simeq 1.5 \times 10^{-6}$ m, respectively. The dependencies of $\langle D \rangle$ on t_d are observed not only for samples 1 and 2 (HH), as in Fig. 3, but also for samples 3–5 (AH). In HH in the range of small t_d, the slopes of the curves are steeper than those of curves obtained for self diffusion of water (Fig. 3). So, with the use of PPO we can observe a transitional regime of self diffusion in HH and AH. The values of D_{eff}/D_0, that characterize permeability of AH for PPO molecules at maximum displacements are given in Table II.

The initial slopes in Fig. 4 also differ. The values of V/S for each of the samples studied were calculated using the approximation given by Equation 8 and are presented in Table II. It is seen from this table that the relations D_{eff}/D_0 for water and PPO are close to each other in all AH samples. This indicates, in particular, that the specifics of the interaction of water and olygomer molecules with the surface of pores is insignificant. So, the curves in Fig. 4 can be considered as an extension of the curves in Fig. 3 to the range of smaller displacements. Taken together, they give a picture of translational molecular mobility in the length scale of $\sim 0.4 \times 10^{-6}$ to $\sim 2.5 \times 10^{-5}$ m, and of peculiarities in the porous structure of the samples under study.

For porous substances of practical interest, like the hardened gypsum, the broad distribution of pore sizes, and the isotropic orientation of pores are typical. Both of these factors result in a distribution of pore projections on the pulsed gradient direction and lead to the distribution of barrier spacing detected by PFG. The minimum barrier spacing represents the pore diameter, and the maximum one represents the pore length. Therefore, the extreme values of RMD corresponding to a transitional regime can be used, in principal, to estimate the minimum diameter and maximum length of pores in the sample.

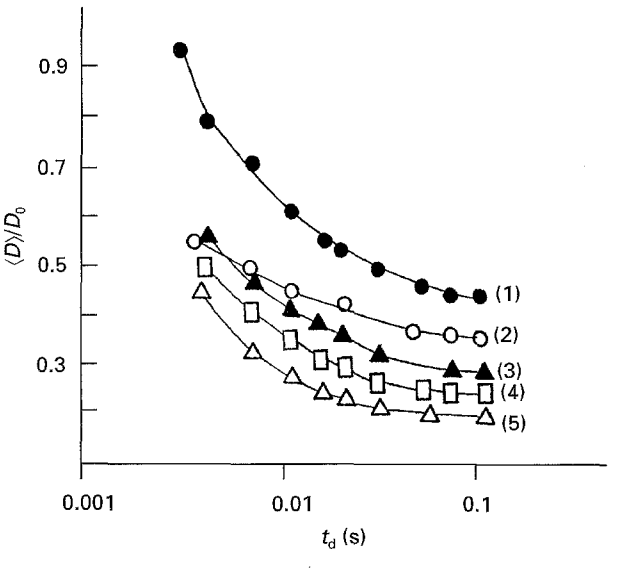

Figure 4 The dependencies of the ratio $\langle D \rangle / D_0$ for PPO molecules as a function of diffusion time for samples (1) 1, (2) 2, (3) 3, (4) 4 and (5) 5 at 10 °C.

Diameters of the pores in most of the samples studied are beyond the resolving power of the PFG method (0.4×10^{-6} m). So, the alternation of liquid diffusion is not determined by the distribution of pore diameters. Evidently it is determined by other dimensions in the scale of RMD, detected by the PFG method. These dimensions can be discussed in terms of the orientation and shape of pores.

The similar shape of EA in all of the samples prepared from HH and AH allows us to conclude that, in these samples, there exist common structural peculiarities of water-confining geometry. The fact that EA can be described by equation 9 [10], shows that the porous systems studied can be considered as a randomly oriented set of layers with respect to the pulsed field gradient. The parts of EA with different slopes correspond to the contributions of the layers with different orientations.

The length scale in which the dependence of $\langle D \rangle$ on t_d is observed includes the whole time scale of water (Fig. 3, curves 1 and 2) and PPO (Fig. 4, curves 1 and 2) (0.4×10^{-6} to 2.5×10^{-5} m) self diffusion. Similar results in HH were obtained earlier for other water to binder ratios [10]. In AH, contrary to HH, the decrease of $\langle D \rangle / D_0$ up to D_{eff}/D_0 is completed at RMD $\sim 0.5 \times 10^{-6}$ m, corresponding to $t_d \sim 20$ ms for PPO self diffusion (Fig. 3, curves 3–5). For all of the AH samples, the plateau is attained at close values of RMD. Consequently, the maximum pore length in AH is about 0.5×10^{-6} m, whereas in HH it is more than $\sim 2.5 \times 10^{-5}$ m. So, the pore sizes are sufficiently greater in HH. The same conclusion follows from the ratio V/S, which is greater in HH, than in AH (Table II). When the structures are similar, the samples with smaller width of the layers are characterized by less permeability. This becomes obvious when we compare the values of D_{eff}/D_0 for HH and AH (Table II).

The modification in all cases causes a decrease in pore diameter (Fig. 1), whereas the shape of EA and RMD, corresponding to the attainment of D_{eff} (Fig. 4), remains constant. Consequently, the similarity of the porous geometry for the samples hardened without and with modifiers, holds. Thus, within the framework of layers geometry, introduced above, the use of modifiers results in a decrease of the layer thickness (pore diameter). The length of the pores remains unaffected. This is in agreement with the decrease in media permeability and in V/S in the samples prepared with modifiers (Table II).

The correlation between compressive strength, P, of the samples (Table I) and characteristics of their porous structure (Table II) is observed. Samples with larger P have the proportionally smaller values of V/S. It is obvious that one of the factors affecting the strength of the sample is the porous structure. Therefore, the NMR method probably could be a useful tool for predicting the mechanical properties of porous substances.

4. Conclusion

The combined analysis of the melting curves of absorbed water and the dependencies of the apparent self diffusion coefficient of water and olygomer on diffusion time, shows that porous geometry of hardened gypsum, prepared from hemihydrate and anhydrite, can be represented by a model of randomly oriented layers. In the case of hemihydrate, more than 95% of pores are arranged in the macropores range. In the case of anhydrite, the fraction of macropores is about 90% and is decreased by the modification to about 30%. The rest of the pores (10%–30%) are arranged in the mesopores range. The latter fact is shown here for the first time for hardened gypsum.

The length of the pores along the layers has been estimated. In the case of hemihydrate this value is more than 2.5×10^{-5} m, and in the case of anhydrite it is about 0.5×10^{-6} m.

It was found that permeability determined from the ratio of the effective self diffusion coefficient to the self diffusion coefficient of the bulk liquid, is essentially less in the case of anhydrite and diminishes in modified samples.

It was determined that the use of modifiers results in decreases in layer thickness and in permeability of hardened gypsum

Acknowledgement

The authors thank V.V. Zhizhenkov, St Petersburgs Joffe Physical-Technical Institute, for helpful discussions. This work was supported in part by Russian Foundation for Fundamental Research grant N95-03-08531a.

References

1. H. BRUKNER (ed.), "Der Baustoff Gips, Stoffliche Grundlagen, Herstellung und Anwendung von Gipsbauelementen" (Veb Verlag fur Bauwesen, Berlin, 1978).
2. I. M. LJASHKEVICH, "Gypsum in Construction Materials" (Vischaja Skola, Minsk, 1989).
3. V. LACK, *Interceram*, **34** (1985) 31.
4. *Idem, Sb. Vut. Brno.* **33** (1984) 87.
5. M. ROSLER and I. OLDER, *Zem. Kalk, Gips*, **42** (1989) 96.
6. S. J. GREGG and K. W. SING, "Adsorption, Surface Area, and Porosity" (Academic Press, London, 1982).
7. G. PAPAVASSILIOU, F. MILIA, M. FARDIS, R. RUMM, E. LAGANAS, O. JAHR, A. SEPE, R. BLINC and M. M. PINTAR, *J. Am. Ceram. Soc.* **76** (1993) 2109.
8. R. BLINC, G. LAHAJNAR, S. ZUMER and M. M. PINTAR, *Phys. Rev. B* **38** (1988) 2873.
9. S. DAVIES and K. J. PACKER, *J. Appl. Phys.* **67** (1990) 3163.
10. A. V. FILIPPOV, E. V. KHOSINA and V. G. KHOSIN, *J. Mater. Sci.* **31** (1996) 1809.
11. S. HAVLIN and D. BEN-AVRAHAM, *Adv. Phys.* **36** (1987) 695.
12. J. KARGER, H. PFEIFER and W. HEINK, *Adv. Magn. Res.* **12** (1989) 1.
13. P. T. CALLAGHAN, "Principles of Nuclear Magnetic Resonance Microscopy" (Clarendon Press, Oxford, 1991).
14. P. P. MITRA, P. N. SEN and L. M. SCHWARTZ, *Phys. Rev. B* **47** (1993) 8161.
15. P. T. CALLAGHAN and O. P. SODERMAN, *J. Phys. Chem.* **87** (1983) 1737.
16. C. CHACHATY, J. P. KORB, J. P. C. VAN DER MAAREL, M. BRAS and P. QUINN, *Phys. Rev. B* **44** (1991) 4778.
17. V. S. RAMACHANDRAN, R. F. FELDMAN and J. J. BEAUDOIN, "Cement Science – Treatise of Current Research" (Heyddn, Chichester, 1981)
18. J. W. GIBBS, "The Collected Works of J. Willard Gibbs" (Academic Press, New York, 1928).
19. W. THOMSON (LORD KELVIN), *Philos. Mag.* **42** (1871) 448.
20. W. A. PATRIC and W. A. KEMPER, *J. Phys. Chem.* **42** (1938) 369.
21. V. A. BAKAEV, V. F. KISELEV and K. G. KRASILNIKOV, *Dokl. Acad. Nauk SSSR* **125** (1959) 831.
22. B. I. VENZEL, E. A. EGOROV, V. V. ZHIZHENKOV and V. D. KLEINER, *Inzh. Fiz. Zh.* **48** (1985) 461.
23. J. H. STRANGE, M. RAHMAN and E. G. SMITH, *Phys. Rev. Lett.* **71** (1993) 3589.
24. S. M. ALNAIMI, J. H. STRANGE and E. G. SMITH, *Magn. Res. Imag.* **12** (1994) 257.
25. A. V. FILIPPOV and D. J. I. IDIJATULLIN, in "Proceedings II, All-Russian Conference "Petrochemistry-94" Kazan, 11–13 October (Technological University, Kazan, 1994) p. 200.
26. E. O. STEJSKAL, *J. Chem. Phys.* **43** (1965) 3597.
27. J. P. TANNER and E. O. STEJSKAL, *ibid.* **49** (1968) 1768
28. V. D. SKIRDA, V. A. SEVRIUGIN and V. I. SUNDUKOV, *Prib. Tekh. Eksp.* **6** (1984) 122.
29. V. P. PRIVALKO, "Structure and Properties of Polymers" (Naukova Dumka, Kiev, 1984).

Received 6 March 1995
and accepted 13 February 1996